Next Energy 8 (2025) 100314

Contents lists available at ScienceDirect

Next Energy

journal homepage: www.sciencedirect.com/journal/next-energy

Research article

P,Fe co-doped $LiMn_2O_4$, a multifunctional material to boost fast charging of lithium-ion batteries assisted by magnetic field

Renier Arabolla Rodríguez[a,b,*], Brandon Frost[b], Jennifer Johnstone-Hack[b,c], Adrian E. Martinez[a], Samia Said[b], Richard I. Walton[d], Eduardo L. Perez Cappe[a], Yodalgis Mosqueda Laffita[a], Paul R. Shearing[e], Dan J.L. Brett[b]

[a] Ionic Conductors Laboratory, Institute of Materials Science and Technology (IMRE), University of Havana, Havana CP 10400, Cuba
[b] Department of Chemical Engineering, Faculty of Engineering Science, University College London (UCL), London WC1E 7JE, United Kingdom
[c] Department of Materials Science and Engineering, University of Sheffield, Sheffield S1 3JD, United Kingdom
[d] Department of Chemistry, University of Warwick, Warwick CV4 7AL, United Kingdom
[e] Department of Engineering Science, ZERO Institute, University of Oxford, Holywell House, Oxford OX2 0ES, United Kingdom

ARTICLE INFO

Keywords:
Multifunctional material
Magnetohydrodynamic effect
Magnetic assisted charging
Lithium batteries
$LiMn_2O_4$ cathode material
Fast charge

ABSTRACT

Fast-charging lithium-ion batteries (LIBs) are essential for enhancing the competitiveness of electric vehicles (EVs) and the rapid charging of consumer electronics. The magnetohydrodynamic (MHD) effect, induced by the Lorentz force acting on moving ions in the electrolyte, has been effectively used to explain the impact of magnetic fields on electrochemical systems. Previous works have shown that when a ferromagnetic electrode in an LIB is exposed to a magnetic field, it is possible to achieve 30% and 50% capacity enhancement and improve its capacity retention. However, generic materials used in the anode or cathode of current batteries exhibit low MHD effects due to their paramagnetic behaviour. This leads to the need to apply large external magnetic fields to witness significant effects, which therefore limits the potential of this technology. To bridge this gap, it is crucial to alter the magnetic behaviour of generic materials used in batteries and systematically study their impact. This research introduces a novel P and Fe co-doped $LiMn_2O_4$ (LMO) material that exhibits ferromagnetism. The developed feature enables the use of low-intensity magnetic fields (33 mT) to control its electrochemical behaviour in an LIB and gain around 25% of capacity. By potentiometric charge/discharge measurements, electrochemical impedance spectroscopy, Atomic Force Microscopy, and COMSOL Multiphysics simulation, it is uncovered the impact of the low-intensity magnetic field on the charge transfer resistance of the cathode and the mitigation of dendrite formation on the anode. This shows the potential of this material in boosting fast charging capabilities and mitigating common degradation issues in LIBs. The study demonstrates how this new material can be a game-changer in the development of more efficient and durable LIBs.

1. Introduction

Fast-charging lithium-ion batteries (LIBs) are fundamental for achieving the competitiveness of electric vehicles (EVs) against traditional internal combustion engine vehicles and facilitating the rapid charge of a diversity of consumer electronic devices. A particular challenge is to meet the established goal of charging EVs in 15 min [1,2], where high-power conditions are required. At present, this is difficult to achieve because under these conditions, degradation occurs in the cathode and inhomogeneous lithium reactions take place in the anode, giving rise to dendrite formation.

External magnetic fields can effectively decrease the polarisation of the cathodes at high current density and mitigate dendrite growth during Li plating/stripping on the anode [3–7]. The magnetohydrodynamic (MHD) effect explains part of the magnetic effects observed in electrochemical systems, such as LIBs. The MHD effect is caused by the influence of the Lorentz force on the ions moving in the electrolyte [5,8]. This effect modifies the current density in an electrochemical cell [5] by creating convective movements in the electrolyte near the electrode surface that decreases the thickness of the diffusion layer and lower polarisation [5]. The dependence of the MHD effect on the

* Corresponding author.
E-mail addresses: renier.arabolla-rodriguez@psi.ch (R.A. Rodríguez), brandon.frost.21@ucl.ac.uk (B. Frost), j.hack@sheffield.ac.uk (J. Johnstone-Hack), adrian.enriquez@imre.uh.cu (A.E. Martinez), samia.said.19@ucl.ac.uk (S. Said), r.i.walton@warwick.ac.uk (R.I. Walton), cappe@imre.uh.cu (E.L. Perez Cappe), yodalgis@imre.uh.cu (Y.M. Laffita), paul.shearing@eng.ox.ac.uk (P.R. Shearing), dan@prosemino.co.uk (D.J.L. Brett).

https://doi.org/10.1016/j.nxener.2025.100314
Received 31 December 2024; Received in revised form 13 April 2025; Accepted 5 May 2025

Lorentz force makes it possible to predict that the stronger the magnetic field, the more intense the MHD effect will become. This allows lower polarisation and higher-capacity gains in cells under the effect of a magnetic field concerning nonmagnetised cells [5]. Another effect of the magnetic field is to change the composition of the CEI and/or SAI by repelling or attracting paramagnetic species near the surface due to the influence of field gradients. Such compositional changes can have a significant impact on the electrochemical performance of the cells in high-power regimes, as reported in the reference [9–11].

Higher magnetic fields can be achieved by using stronger external fields from sources like strong magnets or electromagnets or by using electrode materials with strong magnetisation, as was reported by Ganguly et al. [4]. Unfortunately, the cathode materials typically used, such as $LiMn_2O_4$ (LMO), $LiFePO_4$ (LFP), $LiNi_{0.8}Co_{0.15}Al_{0.05}O_2$ (NCA) or any $LiNi_xMn_yCo_zO_2$ (NMC), present only mild paramagnetic effects. For instance, an investigation using $LiCoO_2$ (LCO) has shown that to achieve substantial improvements in the discharge capacity, a high magnetic field of 1.8 kG (180 mT/18 kOe) must be applied [3]. In that work, the gain of capacity due to the lower polarisation caused by the applied magnetic field increased with the C-rate up to a maximum of ~22% at 5C [3]. Additionally, by applying the magnetic field, lithium plating on the anode, SEI growth, and film fracture were mitigated [3]. As another example, in a nonaqueous iron-vanadium redox flow battery, results showed that a static external magnetic field can reduce the viscosity of the deep eutectic solvent electrolyte, increase the conductivity of the active ions, and improve its electrochemical characteristics [12]. The authors hypothesise that the external magnetic field accelerates the speed of the active ions in the electrolyte [12]. However, to achieve these significant changes, a high magnetic field (100–600 mT/10–60 kOe) also had to be used.

To tackle the low magnetisation of typical battery materials, in a recent work conducted by this team of authors, it was shown that phosphorus and iron doping of $LiMn_2O_4$ (LMO) nanomaterial provides ferromagnetism [13]. That makes this material a first-of-its-class multifunctional material where the electrochemical behaviour of the cell can be controlled by low-intensity magnetic fields (23 mT/230 Oe) [13]. Specifically, this new multifunctional material (called P,Fe_{15}-LMO for simplicity) charges in 13 min and gains between 11 and 15 mA h g^{-1} capacity by only exposing it to a static external magnetic field, which is around 20–25% of its capacity without the magnetic field [13]. By comparison, the percentage of capacity gain in the P,Fe_{15}-LMO is similar to that of the $LiCoO_2$ (LCO), but with a magnetic field 6 times lower and an ionic speed ~4.5 times lower. Furthermore, the investigation of the capacity gains of other generic commercial materials such as $LiNi_{0.5}Mn_{1.5}O_4$ and $LiNi_{0.5}Mn_{0.3}Co_{0.2}O_2$ (NMC 532) in similar conditions to those used for the P,Fe_{15}-LMO revealed maximum capacity gains of only 11% and 8.5%, respectively [13]. This showcases the impact that the new magnetic features of the P,Fe_{15}-LMO have on its electrochemical performances under a static external magnetic field. Thus, performing a systematic study of the mechanism through which the magnetic field influences electrochemical cells using P,Fe_{15}-LMO is needed.

LMO materials are mostly used in batteries for low-cost EVs blended with NMC materials. Blending LMO and NMC seeks to deliver affordable EVs by reducing the amount of Co and Ni in the battery, yet at the expense of a lower capacity and autonomy. Companies such as Samsung SDI, LG Chem, and Li Energy have successfully used this approach [14]. Given the existence of an attractive niche of market blending LMO and NMC cathode materials, it is also paramount to explore how a low static external magnetic field impacts the electrochemical behaviours of a blend between the P,Fe_{15}-LMO and NMC 532 in a high-power regime.

This research work aims to provide first insights into the electrochemical parameters that are modified when a low magnetic field is applied to the ferrimagnetic P and Fe-doped LMO material. The results show the impact that the magnetic field has on the reversible capacity of the materials under a magnetic field, as well as its impact on the lithium dendritic growth on the anode side. Additionally, the work provides insights into key parameters that affect the degradation mechanism of a new ferromagnetic LMO material and its blend with commercial NMC 532 under the influence of a magnetic field.

2. Materials and methods

Phosphorus and iron-doped $LiMn_2O_4$ spinel material (P,Fe_{15}-LMO) were synthesised using a citrate sol-gel method reported previously [15]. Details of the composition, structure, and physical properties of this material can be found in the reference [13]. Briefly, a solid citrate precursor was synthesised containing a Li/transition metal/citrate ratio 1:2:3. The precursor was calcined between 420 and 450 °C to obtain the oxide product. NMC 532 ($LiNi_{0.5}Mn_{0.3}Co_{0.2}O_2$) was purchased from XIAMEN TOB New Energy Technology Co. A blend between P,Fe_{15}-LMO and NMC 532 was prepared ~5 min hand mixing and homogenisation of these materials in a proportion 2:3.

The electrochemical measurements were performed in a battery cycler (BCS-805 Biologic) at room temperature. For the measurements, coin cells were assembled in an Ar-filled glove box. Metallic lithium was used as the anode, $LiPF_6$ (1 M), ethylenecarbonate: dimethylcarbonate (3:7), 2% VC solution was used as the electrolyte, while the cathode electrode was a mixture of the active material, carbon Super Black C65 and PVDF (75:15:10). Aluminium foil was used as the cathode current collector, while the electrolyte was supported in Celgard 2500 separator membrane. Rate capability and capacity retention experiments for the P,Fe_{15}-LMO cathode material were conducted between 3 and 4.47 V. For the blended electrode, the potential window was set between 3 and 4.3 V. All experiments were conducted using a constant current charge/discharge protocol. This aims to accurately study the interaction between the magnetic field and the speed of charge/discharge at different current rates, avoiding the influence that electrode porosity/tortuosity can have on the capacity transient produced in constant current/constant voltage protocols.

To conduct the electrochemical measurements under the influence of a magnetic field, a cylindrical magnet was fixed in the centre of the lower face of a CHH-1 biologic coin cell holder. The magnet had a magnetic field on its surface of 33 mT (330 Oe). The experimental setup is represented in the Electronic Supplementary Information (ESI 1). The magnet had a diameter of $d = 17.74$ mm and a thickness of $h = 5.01$ mm. The gap between the upper surface of the magnet and the electrode was 4.13 mm. The presence of the fixed magnet allows constant exposure of cells during their formation and cycling without the temperature rise stemming from other alternative sources of magnetic field, such as electromagnets or magnetic coils.

Electrochemical impedance spectroscopy (EIS) experiments were carried out at 3 V. The frequency range was 10 mHz to 100 kHz and the voltage perturbation was 5 mV. For EIS spectra fitting the analysis tools of the programme BT-Lab V1.66 were used.

To record images of Li electrodes at different numbers of cycles, atomic force microscopy (AFM) was used. Coin cells were opened in a glove box for their postmortem study. Li electrodes were kept in a glove box to dry. AFM experiments were carried out in an Ar-filled glove box (Mbraun YKG series) with $H_2O < 0.1$ ppm, $O_2 < 0.1$ ppm. The film morphology was characterised using PeakForce quantitative nanomechanical mapping mode with a SCOUT350 silicon probe with reflective Al coating (NuNano, $k = 42\,N\,m^{-1}$, $f_0 = 350$ kHz). Images were collected with 512 samples/lines over a scan area of 5 μm^2. All of the results obtained from the AFM were analysed by Gwydion software.

The simulation of different profiles of the magnetic field for a coin cell with the P,Fe_{15}-LMO material and a hypothetical $LiMn_2O_4$ material was performed in the software COMSOL Multiphysics 4.2 employing the zero current magnetic field modulus. The finite-element method was used to solve the system of Maxwell´s differential equations for the geometry, frontier conditions, and mathematical grid of points. The position of the magnet, coin cell, and holder, as well as the other shape

and magnetic features of the magnet described above, were considered for the simulation. The thickness of the positive electrode was fixed at 0.2 mm. Air, 9Ni Steel (UNS K81340), PVC (40% plasticizer), and $LiMn_2O_4$ were included from the modulus of the programme to simulate the influence of the surrounding, metallic parts (from the coin cell and the holder), plastic parts (from the coin cell holder) and the cathode electrode on the magnetic field. To include the magnetic effect of the phosphorus and iron-doped $LiMn_2O_4$ (P,Fe_{15}-LMO) in the simulation, the magnetic permeability of the $LiMn_2O_4$ was modified. Its value was changed from the standard value at room temperature (μ_{LMO} = 1.00867), to the value that can be calculated ($\mu_{P,Fe15\text{-}LMO}$ = 1.4075) from the magnetic susceptibility measured for the P,Fe_{15}-LMO in our previous work (1.3688 emu mol^{-1} Oe^{-1}) [13].

For visualising the 3D microstructure of the cathodes, samples were prepared for tomography by using an A Series Laser Micromachining System (Oxford Lasers, Oxford, UK) in which discs with a diameter of 2 mm were milled out of a larger sample. The samples were mounted into custom-built holders [16] and stacked on top of each other to allow for multiple recipe points to be set up and sequential scans to be carried out. A Zeiss XRadia 620 Versa (Carl Zeiss Microscopy, Pleasanton, USA) was used to scan all samples. A source voltage of 80 kV and power of 10 W was used in all cases, and scans were collected using 4× optics and 3 s exposure time. After reconstruction using proprietary Zeiss reconstruction software, the resulting datasets had a voxel size of 1 µm. Image processing was done using Avizo (Thermo Fisher Scientific, US) software. Datasets were imported into Avizo, and snapshots of various virtual 'orthoslices' and volumes were extracted to visualise the internal electrode structure of each sample.

3. Results

3.1. Electrochemical study and postmortem observations in P,Fe_{15}-LMO under magnetic field

Structural and magnetic features of the phosphorous and iron-doped LMO (P,Fe_{15}-LMO) nanomaterial can be found in reference [13]. It was established previously that in this material, P sits in a 48f crystalline position [13,17]. In this position, phosphorus seems to induce Fe^{3+} to accommodate in neighbouring octahedral 16c crystalline positions of the LMO spinel structure and potentiates Fe^{3+}-O- (Fe^{3+}/Mn) spin interactions [13]. Such interactions produce a magnetic susceptibility of 1.3688 emu mol^{-1} Oe^{-1} for P,Fe_{15}-LMO at 298 K [13]. This value is around 120 times higher than that for the LMO (0.0116 emu mol^{-1} Oe^{-1}) [13], over 100 times higher than the magnetic susceptibility that can be estimated for a 0.21 mol Fe-doped LMO (0.0133 emu mol^{-1} Oe^{-1}) [18] and also around 125 times higher than the value (0.0110 emu mol^{-1} Oe^{-1}) that can be estimated from a report made for the $LiFe_{0.5}Mn_{1.5}O_4$ spinel oxide [19]. Comparison between the magnetic susceptibility of the P,Fe_{15}-LMO against other materials such as NMC 532 can also be seen in Table 1 ESI3. Such a dramatic increase corresponds to the transformation of the magnetic behaviour of the LMO material from paramagnetic to ferromagnetic when doped.

To investigate the potential of the emerged ferromagnetism, Fig. 1a shows the rate capability of the P,Fe_{15}-LMO when exposed to a static external magnetic field. As observed, a capacity gain (10–12 mA h g^{-1}) between the cell exposed and unexposed to the magnetic field is observed at a cycling rate of 2C. Comparative capacity-gain studies conducted in a previous paper showed that the P,Fe_{15}-LMO presents the highest capacity gains when compared against other similar generic materials showcasing the impact of the developed magnetic features on the rate capability performance [13]. The charge/discharge profile at a 2C rate is presented in Fig. 1b. In general, it is observed that the capacity of the P,Fe-LMO material is lower at C/2 (80 mA h g^{-1}) than expected values (120–130 mA h g^{-1}). This is because, for the doping with P and Fe, Mn^{3+} (the electroactive species) was substituted, and only 64% of it is still present. During the electrode's charge (Fig. 1c), the lower insertion voltage of the cell exposed to the magnetic field facilitates the capacity gain of 10 mA h g^{-1}. Such capacity gain is maintained during the discharge of the cells (Fig. 1b). During the discharge, it can also be observed that when the sample is exposed to the magnetic field, the plateau corresponding to Li^+ insertion within the 2-phase region λ-Mn_2O_4/$Li_{0.5}Mn_2O_4$ is observed. In contrast, for the cells discharged without the magnetic field, polarisation effects seem to hinder this region, and Li^+ insertion takes place mostly within the $Li_{0.5}Mn_2O_4$/$LiMn_2O_4$ 2-phase plateau. A possible explanation to this behaviour could be related to the change of the magnetic behaviour of the P,Fe_{15}-LMO along its charge and discharge. It is possible to hypothesise that changes in its magnetisation over different states of charge can influence the polarisation of the oxide/electrolyte interface; however, proving this will require more thorough research.

On the other hand, at capacity rates lower or superior to 2C, no capacity gains are evidenced. To explain the behaviour observed at low rates (C/2, 1C) and high rates (5C, 10C), the effect of an increasing cycling rate of an electrochemical system exposed to an external magnetic field has to be considered.

At low cycling rate (1C, 2C) the capacity of the cells exposed and not exposed to the external magnetic field are the same. To explain this, it is important to notice that the Lorentz force ($\mathbf{F_L}$) responsible for the MHD effect is proportional to the flux ($\mathbf{J}$) of the charge carriers (Li^+) and the intensity of the magnetic field ($\mathbf{F_L} = \mathbf{J}x\mathbf{B}$) [5,10,20]. This means that

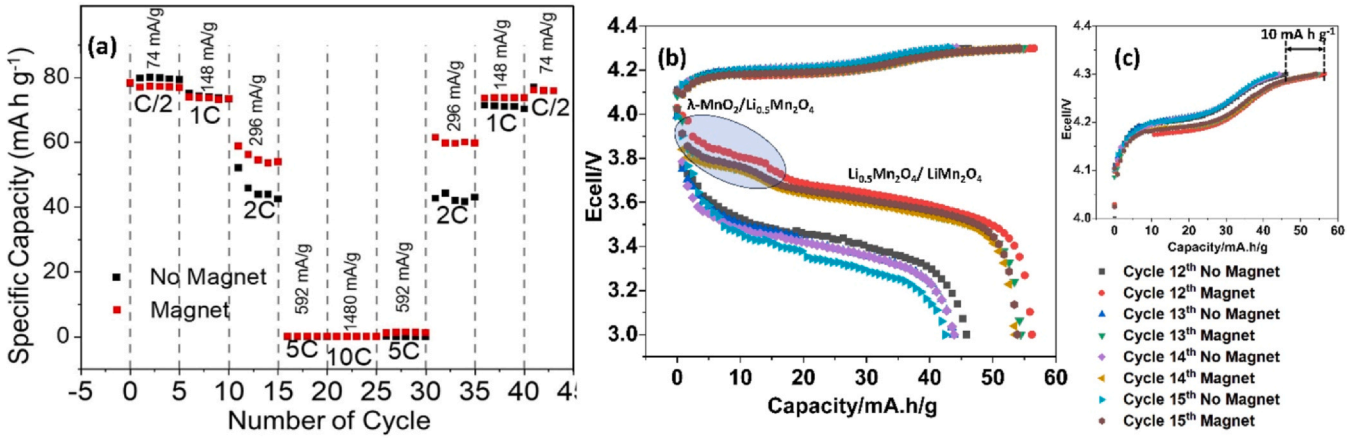

Fig. 1. a) Rate capability characterisation of the P,Fe_{15}-LMO material with no magnet (black squares) and under a magnetic field of 33 mT (330 Oe) (red squares), b) charge and discharge profiles at a cycling rate 2C (296 mA/g) with and without magnetic field, and c) charging voltage profile of the sample when exposed to the magnetic field.

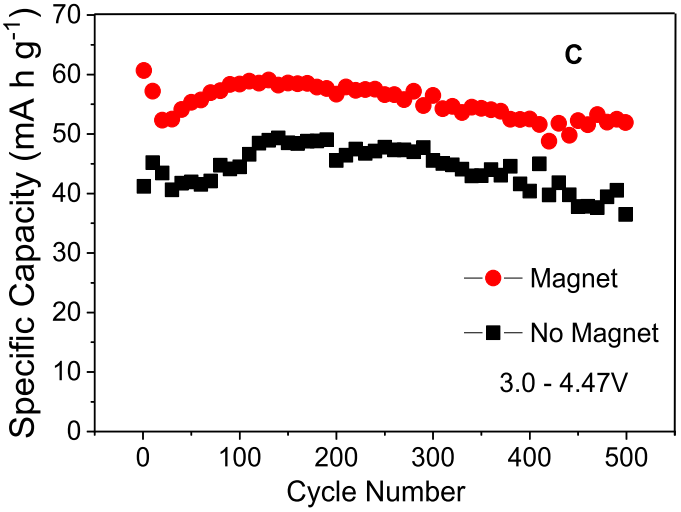

Fig. 2. Capacity retention of the P,Fe_{15}-LMO at 2 C without magnet (black squares) and under the influence of a low magnetic field (33 mT/330 Oe) (red circles).

low or non-MHD effects should be expected at low rates. Therefore, due to the mild MHD effect at these currents, no capacity gain should occur and, consequently, the specific capacity of the cells should match in a reproducible fashion, as observed in Fig. 1.

On the other hand, at higher-capacity rates (5C and 10C) polarisation effects are too high for this material and capacities near 0 mA h g^{-1} are measured. Such polarisation effect can obscure the MHD effect, which explains the poor performance of the system, even after the application of the magnetic field.

An understanding of the effect of a constantly applied magnetic field on the capacity retention of the material in a cell can be seen in Fig. 2. The application of the magnetic field does not considerably change the degradation profile of the cell over 500 cycles, and a constant capacity difference of ~10 mA h g^{-1} is seen between the cell exposed to the magnetic field (red circles) and the nonexposed cell (black squares). In Fig. 1 ESI2, the trend of the point-to-point standard deviation between cells cycled with and without the magnetic field can be observed. As observed, when considering the cell-to-cell variability indicated by the error bars, the average capacity of cells operating with the magnetic field is significantly different from that of cells operating without the magnetic field. The permanence of the capacity gain over several cycles suggests that the Fe^{3+}-O- (Fe^{3+}/Mn) spin interactions in the structure of the material do not suffer considerable changes during cycling. Therefore, the higher value of magnetic susceptibility registered for this material remains, contributing to the total magnetic field across the electrode over many cycles of charge and discharge. Furthermore, it is likely that the interaction between the augmented magnetic field and the ionic flux in the cell governs charge transport and charge transference phenomena near the electrode surface during the cycling process.

To understand the performance of cells under a magnetic field, coin cells cycled with (magnet) and without (no magnet) the influence of the magnetic field were studied by electrochemical impedance spectroscopy after duties of 350 and 500 cycles (Fig. 3).

Fig. 3a shows that after 350 cycles, the charge transference resistance (R_{CT}) of the cell cycled under the magnetic field is almost half the resistance of charge transference for the cell cycled without the magnetic field (Table 1). Given the permanent presence of the magnetic field during formation and cycling up to the 350 cycles, such a difference is likely to be related to the formation of a thinner solid electrolyte interphase (SEI) and cathode electrolyte interphase (CEI) in the anode and cathode, respectively. On the other hand, after 500 cycles, cells cycled with and without the magnetic field show comparable values of the charge transference resistance. This can be explained by considering that in the long term, the growth of the SEI and CEI will be substantial regardless of the influence of the magnetic field. Also, changes in the composition of the CEI due to the influence of magnetic field gradients can impact the resistance of charge transfer after a substantial number of cycles [10].

Regarding capacitive effects, after 350 cycles, the electrode performing under the influence of the magnetic field shows a higher Q_{dl} and a slightly lower time constant (Table 1). This is consistent with the formation of a thinner double-layer under the influence of the magnetic field since a thinner electrochemical double-layer induces a higher capacitive effect (hence Q_{dl} is also higher) with a lower polarisation (lower τ) due to its smaller resistance. In contrast, after 500 cycles, Q_{dl} is lower for the electrode exposed to the magnetic field, but its time constant remains lower (like the case after 350 cycles) compared to the cell not exposed to the field. Such a result is difficult to explain due to the complexity and heterogeneity of the CEI after a high number of cycles. Nonetheless, it could be speculated that after a high number of cycles, although the thickness of the electrochemical double-layer could be comparable or even higher for the electrode exposed to the magnetic field, its chemical composition or morphology still allows faster lithium transport. This assumption is justified by the higher value of the diffusive constant phase elements Q_D for the electrodes exposed to the magnetic field compared to the nonexposed ones (Table 1).

To investigate the influence of the magnetic field on the anode side, optical photos and atomic force microscopy images were recorded of the fresh and postmortem metallic lithium electrodes (Fig. 4).

Fig. 4a shows the surface of a fresh metallic Li electrode. It can be observed in the optical image that the surface of the electrode initially presents a metallic-like colour characteristic of lithium. The AFM image and the reconstruction of the roughness map show a relatively homogeneous surface, characterised by a roughness (RMS) of 39 nm. After 5 cycles of charge/discharge at 2C (Fig. 4b), the optical image of the cycled electrode under a magnetic field shows subtle differences with respect to the electrode that was cycled without the magnetic field. While the electrode not exposed to a magnetic field presents pits and

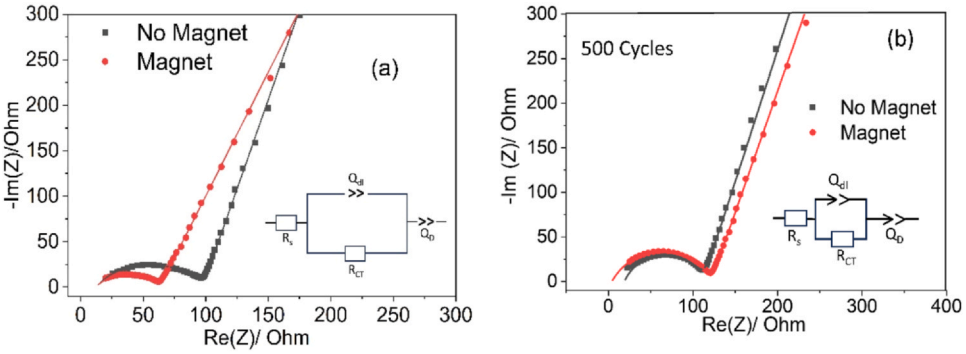

Fig. 3. Electrochemical impedance spectroscopy (EIS) of the cells P,Fe_{15}-LMO versus Li after: a) 350 cycles and b) 500 cycles. The black spectra represent cells cycled without a magnetic field, while the red spectra correspond to cells cycled under a magnetic field of 33 mT (330 Oe). The inset in both figures represents the equivalent circuit used to fit the experimental data. R_s and R_{CT} represent the electrolyte resistance and charge transference resistance, respectively. Q_{dl} and Q_D are constant phase elements used to represent capacitive phenomena in the electrochemical double-layer and diffusive phenomena in the electrode, respectively.

Table 1
Electrokinetic parameters for cells cycled 350 and 500 times with and without the influence of the magnetic field

Cycle Number	Magnetic Field (mT/Oe)	R_{CT} (Ohm)	Q_{dl} $*10^{-5}$ (Fs^{n-1})	n	$\tau = RC$ $\times 10^{-4}$ (s)	$Q_D \times 10^{-3}$ (Fs^{n-1})	n_D
350	0	85 ± 2	3 ± 1	0.6	1.5	2.66 ± 0.05	0.8
	33/330	55 ± 1	8 ± 2	0.6	1.0	5.59 ± 0.08	0.8
500	0	105 ± 2	5 ± 1	0.6	2.4	2.91 ± 0.04	0.8
	33/330	118.9 ± 0.7	1.9 ± 0.2	0.66	1.0	4.5 ± 0.6	0.8

R_{CT} is the charge transference resistance; τ is the characteristic time constant of the RC equivalent circuit; Q_{dl} and Q_D are constant phase elements to represent capacitive phenomena in the electrochemical double-layer and diffusive phenomena in the electrode, respectively; and n and n_D are the exponents relative to Q_{dl} and Q_D.

clear signs of inhomogeneous lithium deposition (region encircled in the image), the electrode exposed to the magnetic field appears smoother. To demonstrate this, roughness maps at a 5 × 5 μm scale were measured on both electrodes (Fig. 4b). As can be observed, the electrode cycled without the magnetic field shows an RMS = 54 nm, superior to that of the fresh Li electrode. Furthermore, the map shows hills and valleys characteristic of the inhomogeneous deposition of Li in certain regions of the electrode at a high cycling rate. In contrast, the electrode exposed to the magnetic field presents an RMS = 17 nm and features a smooth surface without significant hills or valleys.

After 350 cycles, considerable differences are observed between an electrode exposed to the magnetic field and a nonexposed electrode (Fig. 4c). First, the optical images of both electrodes show the formation of a black layer product corresponding to the growth of SEI. However, the AFM images exhibit an irregular surface for the nonexposed electrode, whilst for the magnetically exposed electrode, the surface looks particularly smooth. In-depth details are obtained by observing the map of roughness. The roughness of the nonexposed electrode more than doubles that of the electrode exposed to the magnetic field (Fig. 4c). More remarkably is that the nonexposed electrode shows high and steep 'hills' that grew with prolonged cycling. On the contrary, the electrode cycled under a magnetic field shows small hills and almost flat features that indicate the effective role of the magnetic field in suppressing the growth of dendrites and inhomogeneities during extended cycling (Fig. 4c).

Measurements of electrodes exposed and nonexposed to magnetic fields were conducted after 500 cycles. However, using AFM images it was not possible to accurately measure roughness parameters due to the significant growth of the SEI, as predicted by EIS. Photos of cycled electrodes after 500 cycles are shown in Fig. 2 ESI2.

Several works have provided an explanation for the observed phenomenon based on the MHD effect. In general, it is agreed that the Lorentz force induces a spiral motion of Li ions around the electrode surface under a magnetic field, and this promotes a more homogeneous distribution of Li across the surface [21–24]. This inhibits the growth of dendrites to obtain a uniform and dense lithium layer. Furthermore, by creating an ionic rotatory movement around the surface, the concentration gradient of Li-ion is reduced, which decreases the concentration polarisation and increases mass transference [21–23]. For the current research, the presence of a ferromagnetic material on the cathode side also plays the crucial role of increasing the intensity of the magnetic field near the anode surface. The Lorentz force that provokes the MHD effect is proportional to the intensity of this magnetic field, for a given ionic flux (**J**). Therefore, an enhanced magnetic field on the surface of the anode side could explain why, even for the smaller external magnetic field, it still leads to suppression of dendrite formation after long cycles of charge and discharge.

3.2. Electrochemical characterisation and degradation study of P,Fe_{15}-LMO/NMC 532 blend

The rate capability of the P,Fe_{15}-LMO/NMC 532 blend under the influence of the magnetic field against a no magnetic field, is shown in Fig. 5a. The first feature to notice is that for the blend, capacity gains between 6 and 7 mA h g^{-1} occur for all the cycling rates. This behaviour can be explained by considering 2 factors: First is that the overall capacity gain is the combination of the capacity gains produced in each particular material, as exhibited in Fig. 1 and in Supplementary Information 7 of the reference [13]. Second, the magnetic-induced enhancement in the electrode due to the presence of the P,Fe_{15}-LMO enables amplification of the particular effect on each material in the electrode.

In Fig. 5b, the capacity retention of the blended electrode exposed to the magnetic field is shown in comparison with the nonexposed blend and the nonexposed NMC 532 electrode. At a low cycling rate (C/5) the NMC 532 electrode shows the highest specific capacity due to its higher capability of inserting and disinserting lithium (C_{teo} = 279 mA h g^{-1}) compared with an LMO-type of material (C_{teo} = 148 mA h g^{-1}). Despite the expected sacrifice in capacity being a downside of blending LMO with NMC, the potential niche for low-cobalt/low-cost batteries enhanced by low-intensity magnetic fields justifies exploring the implications of blending NMC 532 with the P,Fe_{15}-LMO.

The blended electrode shows that under the presence of the low magnetic field, at a low cycling rate (C/5, 45.2 mA g^{-1}), it delivers a small capacity increase (~1 mA h g^{-1}) as expected due to the weak influence of the Lorentz force (Fig. 5b). However, important differences are observed when cycled at 2C (452 mA g^{-1}). At this current, the magnetised blended electrode delivers a higher capacity than the blended electrode without the magnetic field. More importantly, although at the beginning (between the 51st and 250th cycle) of cycling at 2C the capacity of the electrode under the magnetic field is still lower than that for the NMC 532 electrode, after the 250th cycle the capacity of the NMC 532 electrode steadily decays while the capacity of the blended electrode remains approximately flat (Fig. 5b). This suggests that if an LMO/NMC blend is to be used for low-cost batteries, an active magnetic material such as the P,Fe_{15}-LMO can play a fundamental role in retarding the degradation of the electrode under the influence of a low magnetic field.

To investigate the role of the magnetic field, the EIS spectrum was recorded for an P,Fe_{15}-LMO/NMC 532 vs Li cell after 500 cycles. Then the same cell was exposed to the magnetic field and the EIS measurement was repeated, the results are shown in Fig. 6a. The confluence of degradation phenomena in both the NMC 532 and the LMO materials makes fitting the system difficult; however, the more visible influence of the magnetic field is on the width of the charge transfer semicircle of both systems.

As can be observed in Fig. 6a, by only allocating the magnetic field near the cell, the charge transfer resistance on the electrode is considerably reduced. This result is crucial because the lower charge transfer resistance reduces the overpotential of the electrode. Such resistance reduction explains that the blended magnet, under the influence of the magnetic field, has a lower degradation profile than those without the magnetic field.

To verify which component of the blended electrode is responsible for the decrease of the charge transference, the EIS spectrum of the NMC 532 was recorded after 500 cycles of charge and discharge

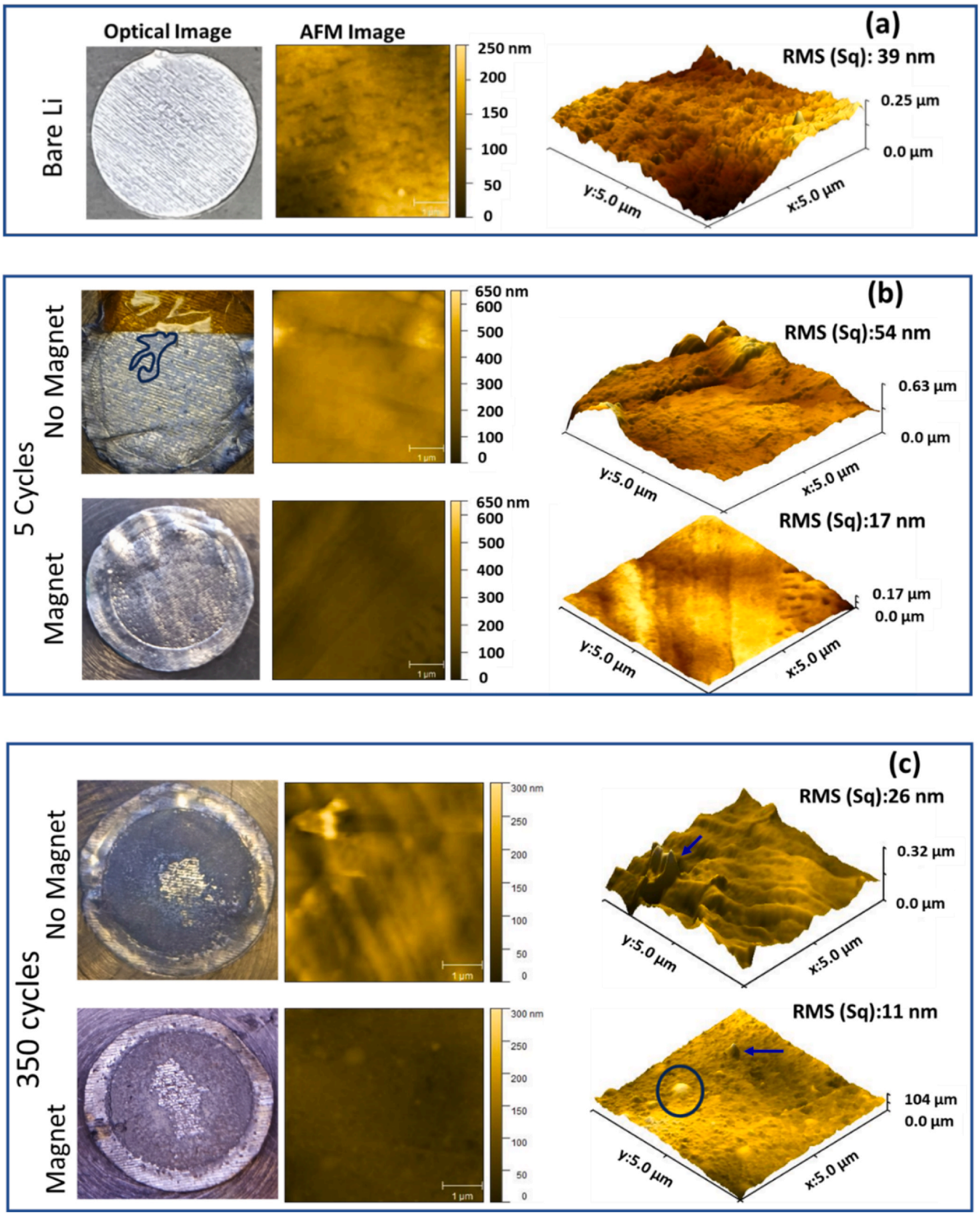

Fig. 4. Optical and AFM images of fresh and postmortem lithium electrodes: a) metallic Li electrode as-received, b) Li electrode after 5 charge/discharge cycles without (top) and with (bottom) magnet, and c) Li electrode after 350 cycles without (top) and with (bottom) magnet.

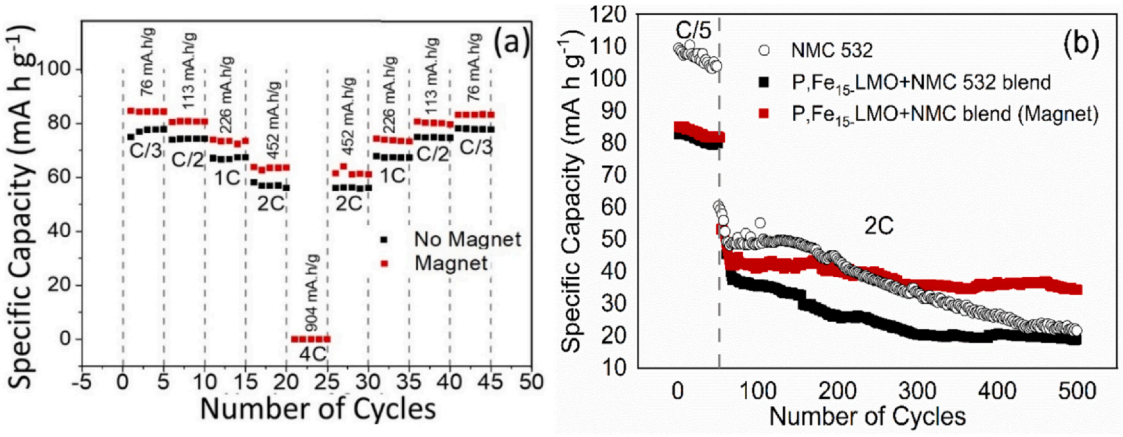

Fig. 5. a) rate capability charge/discharge of the P,Fe-LMO/NMC 532 blended electrode with (red squares) and without (black squares) the influence of a magnetic field of 33 mT, and b) Capacity retention of a NMC 532 electrode (black-outline circles), and the P,Fe-LMO/NMC 532 electrode with (red squares) and without (black squares) the influence of a magnetic field of 33 mT.

(Fig. 6b). Similar to the case of the blended electrode, after 500 cycles, the EIS spectrum was recorded for the same cell with and without the magnetic field. Fig. 6b shows that the magnetic field does not produce significant changes in the total resistance (~30 Ohm) of the electrochemical double-layer. This suggests that the changes observed in the P,Fe_{15}-LMO/NMC 532 blended electrode are mostly influenced by the magnetic field on the ferromagnetic P,Fe_{15}-LMO component of the electrode.

3.3. Simulation

To achieve a closer understanding of the importance of enhancing the magnetic features of the P,Fe_{15}-LMO for the electrochemical Li^+ transport under a magnetic field, Fig. 7 shows characteristics of the magnetic field (MF) across the symmetry plane (**P**) and the lines $\mathbf{L_1}$ (y = 0.1 mm), $\mathbf{L_2}$ (y = 0.2 mm) and $\mathbf{L_3}$ (x = 5.5 mm) (see plane and lines in the inset of Fig. 7). For comparison, the magnetic effects in the P,Fe_{15}-LMO electrode are contrasted against a hypothetical electrode made of paramagnetic phosphorous doped $LiMn_2O_4$ (P-LMO) or NMC 532 materials. The magnetic susceptibility of the different materials is provided in Table 1 ESI3. For visualisation purposes, a 2 mm disc punched for X-ray tomography measurements is used as a representation of the 11 mm electrode used for COMSOL simulations.

In the configuration employed, Electronic Supplementary Information 1 (ESI 1), the strength of the magnetic field is stronger on the borders of the electrode than in the centre. This can be appreciated in the colour maps in Fig. 7a and b. Due to the small thickness of the electrode (0.2 mm), the $\mathbf{L_1}$ line can be used to represent the general trend of the magnetic field inside the ferromagnetic P,Fe_{15}-LMO material and to compare it against what would happen within a paramagnetic material such as the P-LMO. In Fig. 7b can be seen that the modulus of the magnetic field (|B|) in the interior of the P,Fe_{15}-LMO electrode (line $\mathbf{L_1}$, y = 0.1 mm) is significantly larger than that for a conventional P-LMO electrode (Fig. 7a). Similarly, when comparing the trend of |B| from the button to the surface of the electrode (vertical line $\mathbf{L_3}$, x = 5.5 mm) it is observed that the largest values of |B| are found for the P,Fe_{15}-LMO (Fig. 7a and b).

The line $\mathbf{L_2}$ represents the interface between the electrode and the electrolyte. Due to the ferromagnetic character of the P,Fe_{15}-LMO, when comparing the overall trend of the modulus of the magnetic field across the electrode diameter ($\mathbf{L_2}$ line), it is observed that the largest values are found for the electrode made of P,Fe_{15}-LMO, as expected (Fig. 7c).

In Fig. 7d, can be observed the effect of the magnetic field on the trajectory of a Li^+ ion during the charge process. As can be seen, the magnetic field amplified by the P,Fe_{15}-LMO changes dramatically the trajectory of the ion from straight, when no magnetic field is used, to a spiral, when the magnetic field is used. Additionally, in Fig. 7d can be seen that for the P,Fe_{15}-LMO electrode, the XY view of the Li^+ trajectory shows a radius of the spirals much larger than that for electrodes made of paramagnetic materials such as P-LMO or NMC 532. To explain the electrochemical implications of the rotational movement of Li^+ ions in electrodes containing P,Fe_{15}-LMO, the effect that it may cause on the electrode diffusion layer can be considered. Fig. 8 shows a schematic illustration of the process that happens at a local level due to the spinning Li ions.

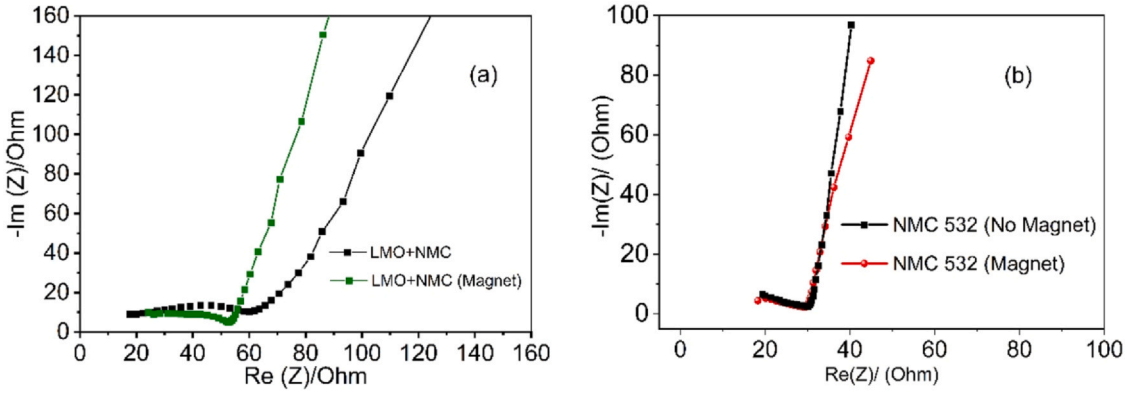

Fig. 6. a) EIS spectra of the blended electrode with (green squares) and without (black squares) magnetic field, and b) EIS spectra of NMC 532 with (red circles) and without (black squares) magnetic field.

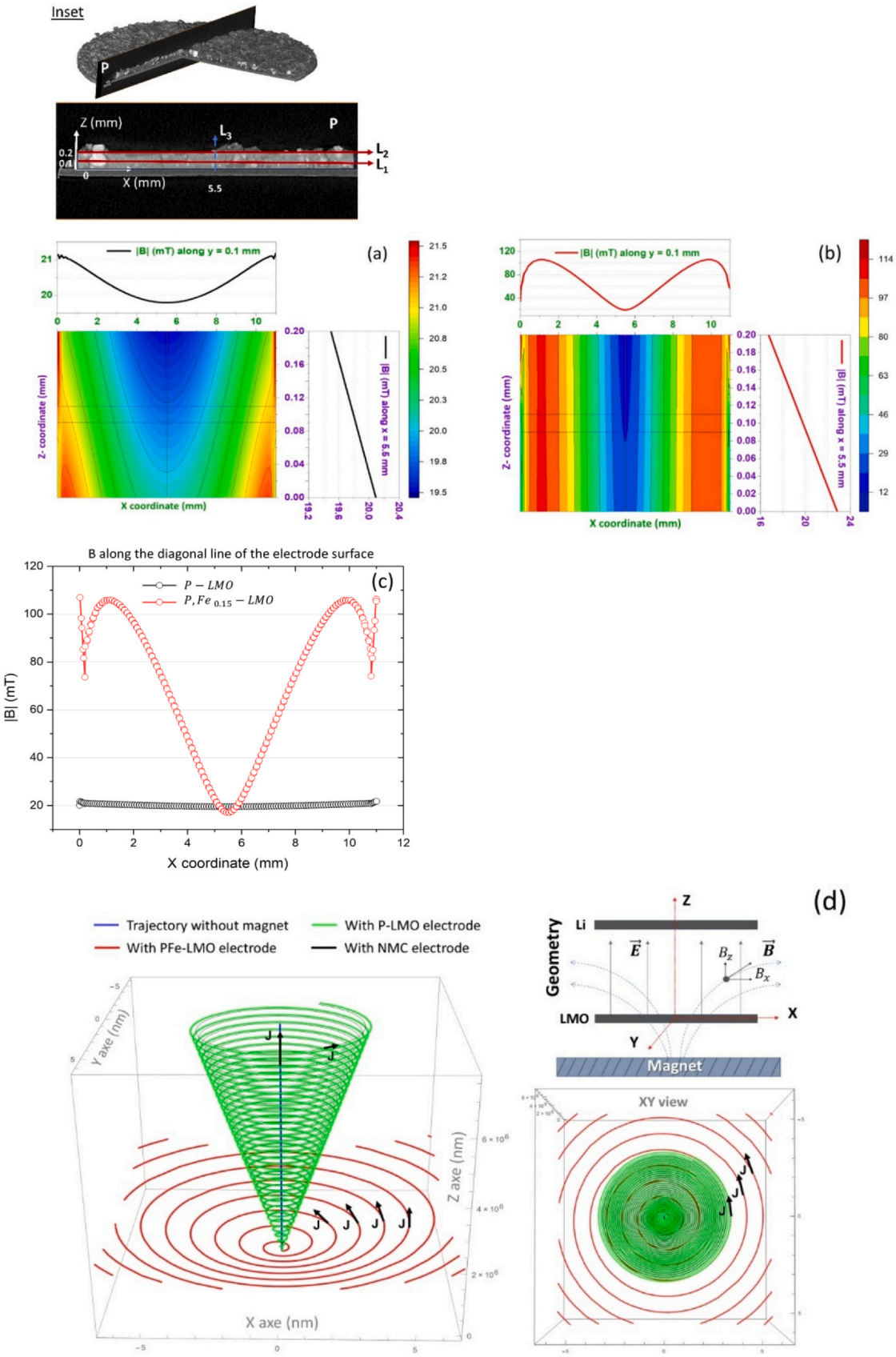

Fig. 7. Colour map of the magnetic field on the cross-section of the electrode (**P** plane): a) Colour map of a hypothetical electrode made of a paramagnetic phosphorus doped LMO (P-LMO) material with magnetic susceptibility $\chi = 0.0116\,\text{emu mol}^{-1}\ \text{Oe}^{-1}$, b) colour map of the P,Fe_{15}-LMO material with $\chi = 1.3688\,\text{emu mol}^{-1}\ \text{Oe}^{-1}$, c) trend of the absolute value of the MF along the electrode surface radial line (**L_2** line), d) trajectories of Li^+ ions under the influence of a 33 mT magnetic field for electrodes made of P-LMO, P,$Fe_{0.15}$-LMO and NMC 532. Inset is an X-ray computed tomography visualisation of the P,Fe_{15}-LMO electrode. Representation of the plane (**P**) and the lines **L_1** (z = 0.1 mm), **L_2** (z = 0.2 mm), and **L_3** (x = 5.5 mm).

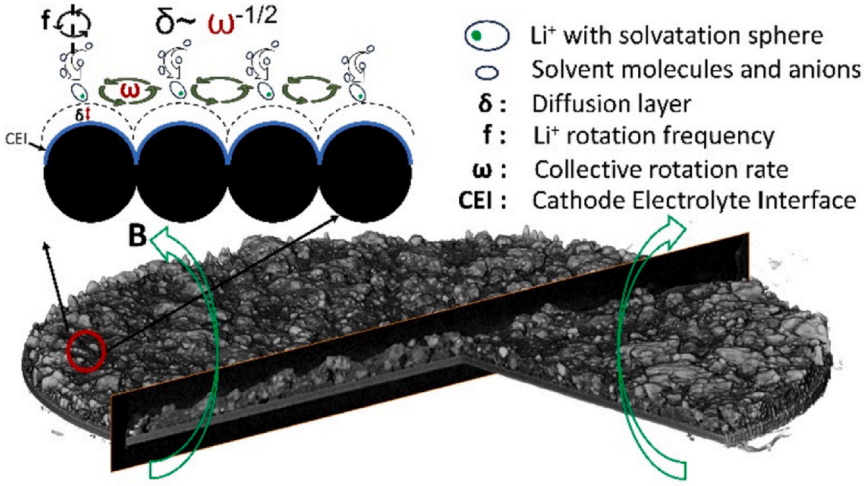

Fig. 8. Illustration of the influence of the magnetic field on the magnetic electrode.

At a local level, Li^+ spins at a frequency '*f*' (schema in Fig. 8) that depends on the x and y coordinates, as exhibited in Fig. 7a and b. When Li^+ is transported through the porous structure of the electrode, it carries between 3 and 4 molecules of the solvent in its first solvation sphere [25,26]. Additionally, in a second coordination sphere, it also transports anions from the electrolyte (PF_6^-) [27]. Without losing generality, it is possible to say that the molecules and ions carried by the Li^+ in motion also drag other molecules of the electrolyte due to the dipole-dipole or ion-dipole interaction. The circular motion of solvated Li^+ ions, together with other ions and molecules of the solvent, is expected to create a locally collective movement of the electrolyte on the surface of the particles at a collective rotation rate 'ω,' Fig. 8.

As established in the electrochemical literature, the thickness of the diffusion layer 'δ' (see Fig. 8) depends inversely on the rotation rate ($\delta \sim \omega^{-1/2}$ [28]). Additionally, we can assume that the electrode behaves more generally as a mixed transport-controlled electrode, where the cathodic current decreases with the diffusion thickness and increases with the charge transfer overpotential [29]. Under these conditions, it can be explained that the increase of the collective rotation rate reduces the diffusion layer, which therefore decreases the charge transfer impedance, as observed in Sections 3.1 and 3.2.

When comparing the effect caused by the P,Fe-LMO with respect to other generic materials such as the NMC 532, it is possible to observe that the radius of the spirals caused by the magnetic effect of the P,Fe-LMO is larger than that for the NMC 532 (Fig. 7d) (XY view). This maximises Li^+ spreading over the electrode surface and the time stirring the electrolyte molecules. The previous effects contribute to homogenise Li^+ concentration and reduce areas of depletion near the anode/cathode surfaces, preventing dendritic growth.

4. Conclusion

The intrinsic magnetic properties of P,$Fe_{0.15}$-LMO are fundamental to lower the electrode polarisation under the influence of small magnetic fields. Because of these properties, it has been observed that the interaction between the flux of Li^+ ions with the augmented magnetic field inside the electrode structure influences the electrokinetic process of charge transfer, even under low magnetic fields. This provokes a reduction in the charge transfer resistance that makes it possible to maintain an approximate capacity gain of 10 mA h g^{-1} over 500 cycles of charge and discharge.

The magnetic field also influences the anode side of the battery. It has been shown that over 350 cycles, the magnetic field considerably reduces the roughness of the surface, decreasing the possibility of dendrite formation. A larger number of cycles thicken the SEI layer, obscuring the effects of the magnetic field. However, the observation realised in this work could find relevance to counteract dendrite formation and the uneven Li plating on graphite anode electrodes.

Blending the P,Fe_{15}-LMO material with higher-capacity cathode materials, such as the NMC 532, proved to be successful in improving capacity and capacity retention of the electrode under magnetic fields. This work has shown that these effects are exclusively due to the presence of the P,Fe_{15}-LMO in the blend. COMSOL simulation helped to explain that in the case of pure P,Fe_{15}-LMO and blended P,Fe_{15}-LMO/NMC 532, the MHD effects caused when Li^+ is transported towards the surface of particles are responsible for the collective agitation of the electrolyte upon the particles surface, reducing Li^+ depletion in the high-power regime which lowers the electrode polarisation. Further experiments are needed to understand the complex behaviour of the formation of the CEI under different magnetic fields, and this will be the subject of future work.

Declaration of Competing Interest

There are no conflicts to declare.

Acknowledgements

The research that gave rise to the results presented in this publication received funds from the Cuban Office of Funds Management and International Projects under the code PN223LH010-40. It is acknowledged that the role of the Caribbean Research and Innovation Collaboration for Knowledge Exchange and Transfer (CRICKET CIC) and the Electrochemical Innovation Lab (EIL) within the Cuba-Britain Energy Network (CuBENet) for providing funds and the facilities to carry out extensive electrochemical characterisation. Jennifer Hack acknowledges the support of the Royal Academy of Engineering under the Research Fellowship programme (EP/T517793/1). Said acknowledges EPSRC Centre for Doctoral Training in the Advanced Characterisation of Materials (EP/S023259/1). Brett and Shearing acknowledge the Royal Academy of Engineering for the financial support of their time (RCSRF2021/13/53 and CiET1718/59). Acknowledgement to the STFC Batteries Network by the STFC Early Career Research Grant (ST/R006873/1).

Appendix A. Supporting information

Supplementary data associated with this article can be found in the online version at doi:10.1016/j.nxener.2025.100314.

References

[1] Goals for High-Performance Batteries for Electric Vehicles (EVs), 〈https://uscar.org/download/245/rfpis/12805/development-of-advanced-high-performance-batteries-for-electric-vehicle-ev-applications.pdf〉.

[2] Battery requirements for future automotive applications. 2019, 〈https://eucar.be/wp-content/uploads/2019/08/20190710-EG-BEV-FCEV-Battery-requirements-FINAL.pdf〉.

[3] A. Sarkar, P. Shrotriya, I.C. Nlebedim, Magnetohydrodynamic control of interfacial degradation in lithium-ion batteries for fast charging applications, ACS Appl. Mater. Interfaces 13 (36) (2021) 43606–43614.

[4] D. Ganguly, et al., Magnetic field assisted high capacity durable Li-ion battery using magnetic α-Fe2O3 nanoparticles decorated expired drug derived N-doped carbon anode, Sci. Rep. 10 (1) (2020) 9945.

[5] C.M. Costa, et al., Magnetically active lithium-ion batteries towards battery performance improvement, iScience 24 (6) (2021) 102691.

[6] F.G. Martin Ebner, Max Kory, Deniz Bozyigit, Method and Apparatus for Applying Magnetic Fields to an Article, Battrion AG, Switzerland, 2021, p. 14.

[7] P.S. Thomas Heenan, Daniel Brett, Chun Tan, Method of Enhancing Electrochemical Cell Performance (Editor), U.B. Limited, UK, 2020.

[8] O. Aaboubi, et al., Magnetic field effects on mass transport, J. Electrochem. Soc. 137 (6) (1990) 1796.

[9] H. Cheng, et al., Emerging era of electrolyte solvation structure and interfacial model in batteries, ACS Energy Lett. 7 (1) (2022) 490–513.

[10] S. Luo, K. Elouarzaki, Z.J. Xu, Electrochemistry in magnetic fields, Angew. Chem. Int. Ed. 61 (27) (2022) e202203564.

[11] Y.-S. Hu, H. Pan, Solvation structures in electrolyte and the interfacial chemistry for Na-ion batteries, ACS Energy Lett. 7 (12) (2022) 4501–4503.

[12] R. Cheng, et al., Effect of exerted magnetic field on the performance of non-aqueous iron-vanadium redox flow battery with deep eutectic solvent (DES) electrolyte, Electrochim. Acta 399 (2021) 139404.

[13] R.A. Rodríguez, et al., P and Fe doping, a strategy to develop light and magnetic responsive multifunctional materials: the case of LiMn2O4, J. Alloy. Compd. 978 (2023) 172837.

[14] M.S.E. Houache, et al., On the current and future outlook of battery chemistries for electric vehicles—mini review, Batteries 8 (2022) 8, https://doi.org/10.3390/batteries8070070.

[15] Y.M.L. Renier Arabolla Rodríguez, Eduado Pérez Cappe, Miguel Angel Aguilar Frutis, J.Santoyo Salazar, Oswaldo Luiz Alves, A new strategy toward enhancing the phosphate doping in $Li_xMn_2O_4$ cathode materials, Ceram. Int. 40 (2014) 12413–12422.

[16] J.J. Bailey, et al., Lab-based X-ray micro-computed tomography coupled with machine-learning segmentation to investigate phosphoric acid leaching in high-temperature polymer electrolyte fuel cells, J. Power Sources 509 (2021) 230347.

[17] R.A. Rodríguez, et al., Impact of phosphorus structural position on the electrochemical enhancement of phosphorus doped LiMn2O4, Electrochim. Acta 337 (2020) 135712.

[18] E. Talik, et al., Electronic structure and magnetic properties of LiMn1.5M0.5O4 (M = Al, Mg, Ni, Fe) and LiMn2O4/TiO2 nanocrystalline electrode materials, J. Solid State Chem. 206 (2013) 257–264.

[19] Y. Li, et al., Structural and magnetic properties of LiMn1.5Fe0.5O4 spinel oxide, Phys. B: Condens. Matter 405 (23) (2010) 4733–4739.

[20] K. Roy, P. Devi, P. Kumar, Magnetic-field induced sustainable electrochemical energy harvesting and storage devices: recent progress, opportunities, and future perspectives, Nano Energy 87 (2021) 106119.

[21] K. Shen, et al., Magnetic field–suppressed lithium dendrite growth for stable lithium-metal batteries, Adv. Energy Mater. 9 (20) (2019) 1900260.

[22] Y. Cao, et al., A novel magnetic coupling to construct spiral deposition of lithium ions for improving anode performance of lithium-sulfur batteries, J. Electrochem. Soc. 168 (3) (2021) 030522.

[23] Y. Chen, et al., Magnetically enhancing diffusion for dendrite-free and long-term stable lithium metal anodes, Green. Energy Environ. 7 (5) (2022) 965–974.

[24] J. Dong, et al., Uniform lithium deposition driven by vertical magnetic field for stable lithium anodes, Solid State Ion. 341 (2019) 115033.

[25] C.-C. Su, et al., Internally referenced DOSY NMR: a novel analytical method in revealing the solution structure of lithium-ion battery electrolytes, J. Phys. Chem. Lett. 9 (13) (2018) 3714–3719.

[26] S.A. Krachkovskiy, et al., Determination of mass transfer parameters and ionic association of LiPF6: organic carbonates solutions, J. Electrochem. Soc. 164 (4) (2017) A912.

[27] B. Ghalami Choobar, et al., Multiscale investigation on electrolyte systems of [(Solvent + Additive) + LiPF6] for application in lithium-ion batteries, J. Phys. Chem. C. 123 (36) (2019) 21913–21930.

[28] G. Denuault, M. Sosna, K.-J. Williams, 11 - Classical experiments, in: C.G. Zoski (Ed.), Handbook of Electrochemistry, Elsevier, Amsterdam, 2007, pp. 431–469.

[29] S. Treimer, A. Tang, D.C. Johnson, A consideration of the application of Koutecký-Levich Plots in the diagnoses of charge-transfer mechanisms at rotated disk electrodes, Electroanalysis 14 (3) (2002) 165–171.